Coupled Interactions at the Ionic Graphene-Water Interface

Anton Robert,[1,*] Hélène Berthoumieux,[2,3,†] and Marie-Laure Bocquet[4,‡]
[1]PASTEUR, Département de chimie, École normale supérieure, Université PSL, CNRS, Sorbonne Université, 75005 Paris, France
[2]Sorbonne Université, CNRS, Laboratoire de Physique Théorique de la Matière Condensée (LPTMC, UMR 7600), F-75005 Paris, France
[3]Fachbereich Physik, Freie Universität Berlin, Arnimallee 14, Berlin 14195, Germany
[4]LPENS, École normale supérieure, Université PSL, CNRS, Sorbonne Université, Université Paris Cité, F-75005 Paris, France

(Received 20 April 2022; accepted 13 January 2023; published 15 February 2023)

We compute ionic free energy adsorption profiles at an aqueous graphene interface by developing a self-consistent approach. To do so, we design a microscopic model for water and put the liquid on an equal footing with the graphene described by its electronic band structure. By evaluating progressively the electronic and dipolar coupled electrostatic interactions, we show that the coupling level including mutual graphene and water screening permits one to recover remarkably the precision of extensive quantum simulations. We further derive the potential of mean force evolution of several alkali cations.

DOI: 10.1103/PhysRevLett.130.076201

The peculiar properties of the water-graphene interface have been unveiled in pioneering experimental [1–3] and theoretical [4–9] studies. This results, in particular, in the extraordinary transport efficiency in water-filled carbon nanotubes and nanochannels [10–12]. Moreover, the presence of charges in the wet nanometric channels leads to exotic ionic behaviors [13–16] that are the cornerstone of energy storage applications [17] and blue energy harvesting [18]. Although experimental data [19,20] regarding specific graphene-ion interactions in water are still few in number, the need to overtake classical molecular dynamics (MD) approximations and to model them at the same level as metal-liquid interfaces [21,22] has been acknowledged. Beyond classical approaches, state-of-the-art quantum calculations combined with solvation codes [23–25] and even fully explicit *ab initio* methods [26,27]—treating both the liquid and the solid at the Born-Oppenheimer level—represent the current state of the art, but their computational cost remains prohibitive for systematic investigations. On the other hand, recent semiclassical numerical studies have described graphene using a perfect metal [28], a Thomas-Fermi [29,30], and an atomistic polarizable force field [21,31] model. Nevertheless, theses studies ignore the semimetallic band structure of graphene. Continuum electrostatic approaches [32,33] permit one to evaluate the well-known attractive "image-charge" electrostatic potential in a dielectric medium. Spatial correlations of both the fluid and the metal can *a priori* be included [34–36] to investigate microscopic effects. However, the self-consistent electrostatic problem is not yet addressed, and collective interactions between electrons and molecules in the liquid are only partially and phenomenologically taken into account.

In this Letter, we develop a quantum and classical field framework to investigate electrostatic interactions at the aqueous graphene interface. We propose a microscopic model for the nonlocal dielectric properties of bulk and interfacial water and compute the polarization function of graphene from a tight-binding model. We evaluate the response function of a nanometric slab of water confined between two graphene sheets by including gradually coupled electrostatic interactions between the electrons of the semimetal and the water molecules. This allows us to derive an accurate evolution of the potential of mean force (PMF) for a single cation solvated in the graphene channel. Finally, we explore the as-derived PMF profiles of a few alkali ions.

Theoretical framework.—Our framework, detailed in Supplemental Material Sec. 1 [37], takes roots in quantum field theory and uses Feynman diagrammatics to derive the Green's function of the interfacial system. As predicted by quantum chemical calculations, the graphene-water interface presents a negligible electronic corrugation [5] and is chemically inactive with no mixing of electronic states [7,38]. We focus on building the nonlocal linear response functions χ of the system, that relate the mean induced charge density $\langle n_{\mathrm{ind}}\rangle$ to an external electrostatic potential ϕ_{ext} generated by a charge distribution n_{ext}. The generic equations used to build the Green's function w of the system and, therefore, the mean electrostatic potential $\langle\phi_{\mathrm{tot}}\rangle$ can be summarized as follows:

$$\begin{aligned} \phi_{\mathrm{ext}} &= v * n_{\mathrm{ext}}, & \langle n_{\mathrm{ind}}\rangle &= \chi * \phi_{\mathrm{ext}}, \\ w &= v + v * \chi * v, & \langle\phi_{\mathrm{tot}}\rangle &= w * n_{\mathrm{ext}}, \end{aligned} \tag{1}$$

where v can denote the bare ($v = 1/4\pi\epsilon_0 x$, with x the distance in 3D space) or an effective Coulomb potential and $*$ the spatial convolution. The starting assumption to build χ is to consider that particles are independent and to derive an *noninteracting* response function $\chi^{(0)}$. Next, $\chi^{(0)}$ is renormalized by considering interactions at the mean-field level: Independent particles respond to the external potential plus the mean polarization potential $\langle\phi_{\rm pol}\rangle$ of the other similar particles. The induced charge density thus reads $\langle n_{\rm ind}\rangle = \chi^{(0)} * [\phi_{\rm ext} + \langle\phi_{\rm pol}\rangle]$ with $\langle\phi_{\rm pol}\rangle = v_{\rm inter} * \langle n_{\rm ind}\rangle$ and where $v_{\rm inter}$ is the effective interparticle potential. This recursive equation combined with Eq. (1) gives

$$\chi = \chi^{(0)} + \chi^{(0)} * v_{\rm inter} * \chi. \tag{2}$$

Equation (1) and (2) sets of equations give the definition for $v_{\rm inter}$ and are used in the following to build the response function of the water (χ_w) and the electronic (χ_e) part separately but also to build χ or w of the entire interfacial system (see Supplemental Material Sec. 2.2 [37], which includes Refs. [39,40]). The interfacial system consists of a channel of nanometric height L made of two graphene sheets and filled with water.

Water bulk.—We now build the response function χ_w of bulk water. Using Eq. (2), the effective electrostatic potential in bulk water $v_{\rm inter} = v_w^{\rm eff}$ can be written $v_w^{\rm eff}(k) = 1/\chi_w^{(0)}(k) - 1/\chi(k)$, with $k = |\mathbf{k}|$. The fluctuation-dissipation theorem gives $\chi_w^{(0)}(k) = -\beta S_w^{(0)}(k)$, where $\beta = 1/k_B T$ and $S_w^{(0)}(k)$ is the single-molecule—or "self-"—charge structure factor, and $\chi_w(k) = -\beta S_w(k)$, where $S_w(k)$ is the charge structure factor of the liquid. Here, we apply this framework to the widely used three-point-charge model of water, SPC/E [41]. The analytical expression of $S_w^{(0)}(k)$ is given in Supplemental Material Sec. 3.1.1 [37], which includes Refs. [41–43]. $\chi(k)$ can be computed in a MD simulation—e.g., the results of Ref. [44] computing the polarization response function $\bar{\chi}_w = -\chi_w(k)/\epsilon_0 k^2$ that are reported in Fig. 1(a). The sharp peak of $\bar{\chi}_w(k)$ centered at $k \simeq 3$ Å illustrates the nonlocal and overscreening properties of water [45].

From the numerical knowledge of the effective Coulomb potential for water $v_w^{\rm eff}(k)$, we suggest the following ansatz:

$$v_w^{\rm eff}(k) = \frac{1}{\epsilon_0 \varepsilon_w^{\rm eff}} \left(\frac{1}{k^2} - \frac{1}{k^2 + \kappa^2} - \frac{\gamma e^{-k^2/2\kappa^2}}{\kappa^2 \sqrt{2\pi}} \right), \tag{3}$$

with the inverse screening length κ, the prefactor γ, and the effective permittivity $\varepsilon_w^{\rm eff}$ as parameters. The last one is fixed to recover the bulk dielectric permittivity of SPC/E water and can be expressed as a function of the molecular dipole moment and bulk density of the fluid. The values of (κ, γ) are adjusted to reproduce the position and the amplitude of the overscreening peak of $\bar{\chi}_w$. The ansatz

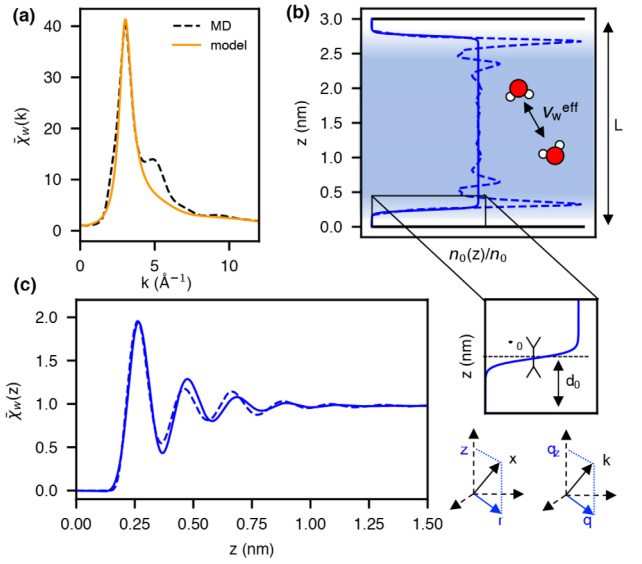

FIG. 1. Dielectric response functions of water. (a) Susceptibility of SPC/E water obtained with MD [44] and with the theoretical model for $\epsilon_w^{\rm eff} = 1.04$ (see Supplemental Material Sec. 3.1.2 [37]), $\kappa = 1.65$ Å^{-1}, and $\gamma = 0.99$. We show the dimensionless quantities $\bar{\chi}(k) = -\chi(k)/\epsilon_0 k^2$. (b) Schematic drawing of the water slab and of the two considered molecular density profiles $n_0(z)$ for $L = 3$ nm. The inset shows the two parameters of the smoothed step function model for $n_0(z)$: d_0 and σ_0. (c) Local dielectric susceptibility $\bar{\chi}_w(z)$ of the slab $P_z = \bar{\chi}_w(z) D_z$ corresponding to the two molecular profiles $n_0(z)$ in (b).

ensures $\chi_w(k) \to \chi_w^{(0)}(k)$ for $k \to \infty$ (see details in Supplemental Material Sec. 3.1.2 [37]).

We plot the polarization response function derived from our framework: $\bar{\chi}_w(k) = -[1/\chi_w^{(0)}(k) - v_w^{\rm eff}(k)]^{-1}/k^2\epsilon_0$ [orange curve, Fig. 1(a)]. Our model captures nicely the dielectric properties of bulk water at low k.

Water slab.—We turn to the dielectric response of a water slab confined between two infinite flat interfaces in the (x, y) plane located in $z = 0$ and $z = L$, respectively [see the sketch in Fig. 1(b)]. We describe the system using cylindrical coordinates in real and Fourier spaces, $\mathbf{x} = (\mathbf{r}, z)$ with $\mathbf{r}$ lying in the interfacial plane and $\mathbf{k} = (\mathbf{q}, q_z)$ with q the in-plane Fourier component [see Fig. 1(c), right]. According to the in-plane invariance, the response function can be written as $\chi_w(q, z, z')$. We show in Supplemental Material Sec. 3.2.1 [37] that we can write

$$\chi_w^{(0)}(q, z, z') \simeq -\beta \frac{\sqrt{n_0(z) n_0(z')}}{n_0} S_w^{(0)}(q, |z - z'|), \tag{4}$$

where $S_w^{(0)}(q, |z - z'|) = \int \frac{dq_z}{2\pi} e^{iq_z|z-z'|} S_w^{(0)}(k)$ and $n_0(z)$ is the molecular density profile that converges to bulk density n_0 in the middle of the channel [see Fig. 1(b)]. We assume that the water molecules interact in the slab between themselves as in bulk, so the slab-geometry effective potential $v_w^{\rm eff}(q, |z - z'|)$ can be obtained by

Fourier transforming Eq. (3) (see Supplemental Material Sec. 3.2.2 [37]). To inverse Eq. (2) and carry out all subsequent computations, we resort to matrix multiplications in the discretized space along z and z'. The (i,j)th element of the matrix $M[z_i, z'_j]$ is given by the function $m(q, z_i, z'_j)$. The solution of Eq. (2) reads $X = [1 - X^{(0)} V_{\text{inter}} (dz)^2]^{-1} X^{(0)}$, where $dz = 0.02$ Å is the grid spacing and where a matrix of size $\lfloor L/dz \rfloor^2$ has been inverted.

We now derive the local dielectric susceptibility $\bar{\chi}_w(z)$, relating the response polarization field P_z to a constant excitation $\mathbf{D} = D_z \mathbf{e}_z$ such that $P_z(z) = \bar{\chi}_w(z) D_z$. We show in Supplemental Material Sec. 4.1 [37] that

$$\bar{\chi}_w(z) = 1 - \frac{d}{dz}\left[\int_0^L dz' \varepsilon_w^{-1}(q \to 0, z, z') z'\right], \quad (5)$$

with $w_w = \varepsilon_w^{-1} * v = v + v * \chi_w * v$, and w_w is the Green's function of the water slab alone, according to Eq. (1).

The slab water density profile $n_0(z)$, which describes the interaction between water and graphene, is an input of the model [see Eq. (4)]. We first consider a generic smoothed step function model, which captures the vacuum layer between the fluid and a surface (encoded by d_0) and the width (σ_0) of the fluid interface [inset in Fig. 1(b)]. In agreement with previous results [8,46,47], the susceptibility calculated in this framework [solid line in Fig. 1(c)] presents an alternation of overresponding [$\bar{\chi}_w(z) > \chi_b$] and underresponding [$\bar{\chi}_w(z) < \chi_b$] layers before reaching its bulk value $\chi_b = 1 - 1/\varepsilon_w$ for $z > 1.25$ nm. Refining $n_0(z)$ by extracting the hydrogen molecular density from a MD simulation [9] using Lennard-Jones parameters by Werder *et al.* [48] [see Fig. 1(b)] induces minor modifications in $\bar{\chi}_w(z)$ [dotted line in Fig. 1(c)]. This first result validates our analytical microscopic model for confined water.

Graphene sheet.—Regarding the solid phase, the noninteracting response function $\chi_e^{(0)}$ can be computed, and we choose a tight-binding model defined elsewhere [49]. Single-particle wave functions $\psi_{\nu,\mathbf{p}}(\mathbf{x})$ and corresponding eigenenergies $\epsilon_{\nu,\mathbf{p}}$ are labeled with the band index ν and the in-plane wave vector $\mathbf{p}$. For one graphene sheet, assuming the small spatial extent of the p_z carbon orbitals, we consider the two-dimensional susceptibility $\chi_e^{(0)}(q, z, z') = \chi_e^{(0)}(q)\delta(z)\delta(z')$, where $\chi_e^{(0)}$ is (minus) the two-dimensional polarizability given by the bare bubble diagram [50]:

$$\chi_e^{(0)}(q) = \frac{2}{\mathcal{A}} \sum_{\nu,\mu,\mathbf{p}} |\lambda^{\nu,\mu}_{\mathbf{p},\mathbf{p}+\mathbf{q}}|^2 \frac{n_F(\epsilon_{\mu,\mathbf{p}+\mathbf{q}}) - n_F(\epsilon_{\nu,\mathbf{p}})}{\epsilon_{\mu,\mathbf{p}+\mathbf{q}} - \epsilon_{\nu,\mathbf{p}}}, \quad (6)$$

where $\mathcal{A}$ is the surface area, n_F the Fermi-Dirac distribution, and $\lambda^{\nu,\mu}_{\mathbf{p},\mathbf{p}+\mathbf{q}} = \int d\mathbf{x} \psi^*_{\nu,\mathbf{p}}(\mathbf{x}) \psi_{\mu,\mathbf{p}+\mathbf{q}}(\mathbf{x}) e^{-i\mathbf{q}.\mathbf{r}}$. We compute Eq. (6) analytically at $T = 0$ K [51] (see result in Supplemental Material Sec. 5.1 [37]) and use a Fermi level of $E_F = k_B T$ to include a minimal number of free electrons.

The response function χ_e is built from Eq. (2) using the bare Coulomb potential for the electron-electron interacting potential, $v_{\text{inter}} = v$, which corresponds to the well-known random-phase approximation [52] (see Supplemental Material Sec. 5.2 [37]). The case of two interacting graphene sheets is detailed in Supplemental Material Sec. 5.2 [37].

PMF modeling and coupled interactions.—Turning to the computation of the PMF, we first derive the Coulomb energy at a mean-field level defined as

$$F(z) = \frac{1}{2} \iint d\mathbf{x} d\mathbf{x}' n_{\text{ext}}(\mathbf{x}) \Delta w(\mathbf{x}, \mathbf{x}') n_{\text{ext}}(\mathbf{x}'), \quad (7)$$

where $\Delta w = w - v$. A spherical test charge of radius b is placed in the channel at the altitude $\mathbf{x} = (0, 0, z)$ such that $n_{\text{ext}}(\mathbf{x}) = \pm e\delta(b - |\mathbf{x} - z\mathbf{e}_z|)/4\pi b^2$. The test charge region is assumed to respond as water. We define the PMF as $\Delta F(z) = F(z) - F(L/2)$. It thus contains only electrostatic contributions and neglects the short-range van der Waals interactions. We now gradually introduce coupled interactions in three steps labeled uncoupled, semicoupled, and fully coupled to build w from the knowledge of χ_e and χ_w.

Figure 2 reports the computed Feynman diagrams and the sketched coupling scenarios. First, we consider the uncoupled case, where water and graphene are blind to each other such that w is clearly separable:

$$w_{\text{uncoupled}} = w_w + v * \chi_e * v. \quad (8)$$

Second, we consider the semicoupled scenario where the polarization charge on the graphene surface results from the potential exerted by the ion and surrounding water molecules. This is the sum of the bare ionic potential and the one induced by the solvating structure of dipoles, that is, the screened potential that is obtained by the water slab Green's function w_w, and, therefore,

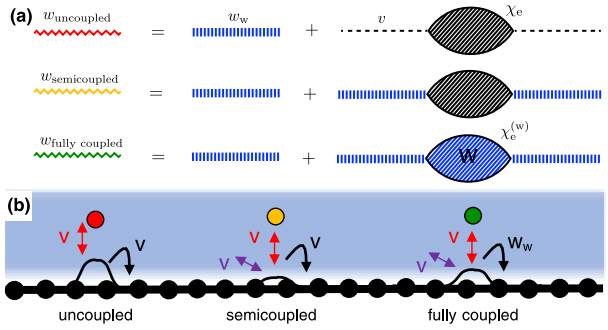

FIG. 2. (a) Computed Feynman diagrams included in the Green's functions for various approximations. The colors of w match the one of curves in Fig. 3. The dashed line represents the Coulomb potential. The hatched bubble diagram depicts χ_e. (b) Schematic illustration of the screening in the different cases (see the text for interpretation).

$$w_{\text{semicoupled}} = w_w + w_w * \chi_e * w_w. \tag{9}$$

It is equivalent to an interfacial semiclassical simulation adding a self-consistent optimization of the surface polarization at each time step, taking into account fixed—and equal to their values in vacuum—site-site interactions of the atomistic model of the metal. For analytical approaches, it corresponds to the ion-metal electrostatic interaction derived in the pioneering work of Vorotyntsev and Kornyshev [34] and later [53]. Finally, the last fully coupled case unveils the presence of the polar liquid for electrons of the solid. Electron-electron interactions are effectively modified due to the presence of water, so that we introduce the *in situ* response function of the metal $\chi_e^{(w)}$ which is built from Eq. (2) with $v_{\text{inter}} = w_w$. Note that this coupling effect cannot be included in a simple way in the standard approaches [34,53]. The most refined Green's function systems, therefore, read

$$w_{\text{fully coupled}} = w_w + w_w * \chi_e^{(w)} * w_w. \tag{10}$$

With the above w expressions, three different PMFs can be computed using Eq. (7). Note that the double integration of Eq. (7) is made in Fourier space and by matrix multiplication [54]. We compute all the PMFs for $L = 6$ nm and using the first density model for $n_0(z)$ with $\sigma_0 = 0.3$ Å [8]. The microscopic distance d_0 is determined by imposing the long-wavelength limit of the surface charge structure factor of water at the interface [9] and equals $d_0 = 1.3$ Å.

To gain insights on the electronic and water contributions to the PMF, we decompose the free energy contribution into two terms: $F = F_e + F_w$, where F_w contains the contribution of water as in an air-water interface replacing w with w_w in Eq. (7). We could consider other substrates by changing $\chi_e^{(0)}$ in Eq. (6).

Results and discussions.—Figure 3(a) displays the resulting different computed profiles for ΔF for one single positive charge of radius $b = 2$ Å, together with a reference curve computed recently from an *ab initio* molecular dynamics (AIMD) study, for K^+ solvated in a 2-nm-thick water slab on graphene [27]. In the AIMD simulation, the limited thickness of the water slab induces a second water-air interface, explaining the nonmonotonic and repulsive *ab initio* PMF behavior above 1 nm. This large range of graphene-water distance ($1 < z < 2$ nm) is not meaningful here. Hence, for the sake of comparison, we shift the *ab initio* PMF such that it is vanishing in the middle of the water slab, for z around 1 nm [black dots, Fig. 3(a)]. The water contribution ΔF_w shows the expected repulsive behavior of the ion at an air interface [blue curve, Fig. 3(a)]. Concerning the water-graphene interface, the uncoupled PMF profile [red curve, Fig. 3(a)] is strongly attractive and presents oscillations with small amplitudes near the surface

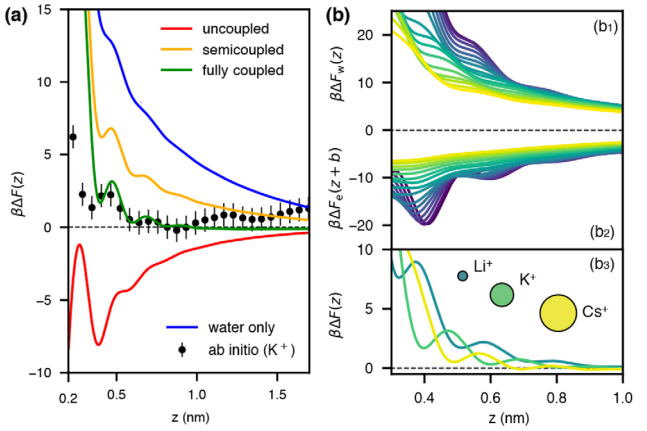

FIG. 3. (a) PMF of K^+ ($b = 2$ Å) at the graphene-water interface. Models with increasing coupling (solid lines) compared to a graphene-free model (blue line) and *ab initio* simulations [27] (black dots with error bars). (b) Detailed contributions to the PMF from water (b_1) and from graphene (b_2) with increasing ionic radius from point charge (blue) to large radius (yellow). For ΔF_e, the ionic center is placed at increasing altitude $\mathbf{x} = (0, 0, z + b)$ for increasing radius. (b_3) Comparative PMF for three alkali ions. The PMF for Li^+ (respectively, Cs^+) is obtained using $b = 1$ Å (respectively, $b = 3$ Å).

stemming from the nonlocal dielectric response of water. Moreover, it deviates a lot from the *ab initio* plot.

Moving to the semicoupled PMF profile [orange curve, Fig. 3(a)], its energy position is shifted to positive values fingerprinting a long-range repulsion and a net reduction of the graphene-ion interaction due to surrounding water molecules. Interestingly, this result is in quantitative agreement with semiclassical simulations [21,28,55] using *ad hoc* surface polarization models (Supplemental Material Sec. 6.2 [37]).

Finally, the fully coupled PMF curve [green curve in Fig. 3(a)] reveals a reamplification of the wall-ion attraction by several thermal energy units and matches almost quantitatively the *ab initio* PMF. This is the key finding of our approach. The nice agreement suggests that this semianalytical approach incorporating electrostatics in a self-consistent way is able to reproduce some key features of the state-of-art reference PMF like the position and amplitude of the three local minima. The stabilizing effect present in the fully coupled case can be qualitatively understood as follows. The absence of repulsive interaction between charge carriers would make them accumulate to one point in order to screen the ionic potential. Thanks to electron-electron interactions, a finite polarization charge can accumulate on the surface as shown by the uncoupled case cartoon in Fig. 2(b). Water molecules actually screen the ionic potential and reduce the polarization charge [semicoupled case, Fig. 2(b)], but in the last fully coupled case, the presence of water effectively reduces electron-electron interactions—by roughly a factor of $(\varepsilon_w + 1)/2$ for electrons that are far apart as shown in Supplemental

Material Sec. 6.3 [37]. As a result, the polarization charge gets reamplified and so does the surface-ion screened potential. The plots differ significantly at short distance, $z < 0.5$ nm, where nonelectrostatic contributions of the PMF—not considered here—are dominant [33].

We now investigate the variations of the PMF with varying radius b ranging from point charge to 3 Å with detailed contributions from water and graphene. Figure 3 (b_1) shows that water repels more strongly smaller ions from the interface. This can be understood by considering the hydrated radius of the cations—defined in continuous theories as the range on which the ion polarizes the surrounding fluid—that is inversely proportional to the ionic radius [56]. Coming from the bulk, Li^+ is the first to break its solvation shell. Figure 3(b_2) compares the nonmonotonic surface contribution ΔF_e for the series of ions, which center is shifted so that the available space for water molecules between ion and surface is equal for each ion. We link the increasing attraction for smaller radii to the ordering degree of the hydration shells as follows. In the limit of poorly structured hydration shells—e.g., for Cs^+—we find the monotonic surface-ion potential of an attenuated charge in vacuum. The opposite limit is a point charge with three highly ordered hydration shells. This gives rise to three special places where icelike water, with a low permittivity, is practically transparent to the potential stemming from the polarization charge on the graphene surface. Summing both contributions in Fig. 3(b_3) for three cations in the alkali series leads to complex PMF profiles. We observe that for increasing radius the three local minima are stabilized in energy, in agreement with an increased capacitance [20] and a reduced hydration energy [24]. Indeed, small ions like Li^+ manifest a strong solvation environment difficult to break hampering its adsorption. Proceeding down the series, Cs^+ yields a weak solvation shell which can be easily desolvated at the graphene interface.

Conclusion.—In this Letter, we build a self-consistent theoretical framework which permits one to investigate analytically the single ionic adsorption at the graphene-water interface. By including the semimetallic band structure of graphene, building a microscopic model for interfacial water, and considering the mutual screening of the two materials, we obtained results that are in excellent agreement with expensive quantum free energy perturbation methods, at a negligible computational cost. Our PMF predictions for the alkali series are in agreement with experimental observations and permit one to distinguish the liquid water and graphene surface contributions. We hope that this versatile and generalizable method will renew some interest in semianalytical approaches and be used to investigate more complex systems involving, for example, ion-ion interactions in nanochannels.

Our code is freely available in the GitHub repository [57].

A. R. thanks D. Borgis for discussions. A. R. and M.-L. B. acknowledge funding from EU H2020 Framework Programme/ERC Advanced Grant Agreement No. 785911-Shadoks. H. B. acknowledges funding from Humboldt Research Fellowship Programme for Experienced Researchers.

*anton.robert@ens.fr
†helene.berthoumieux@sorbonne-universite.fr
‡marie-laure.bocquet@ens.fr

[1] B. Radha, A. Esfandiar, F. C. Wang, A. P. Rooney, K. Gopinadhan, A. Keerthi, A. Mishchenko, A. Janardanan, P. Blake, L. Fumagalli, M. Lozada-Hidalgo, S. Garaj, S. J. Haigh, I. V. Grigorieva, H. A. Wu, and A. K. Geim, Nature (London) **538**, 222 (2016).
[2] E. Secchi, S. Marbach, A. Niguès, D. Stein, A. Siria, and L. Bocquet, Nature (London) **537**, 210 (2016).
[3] L. Fumagalli, A. Esfandiar, R. Fabregas, S. Hu, P. Ares, A. Janardanan, Q. Yang, B. Radha, T. Taniguchi, K. Watanabe, G. Gomila, K. S. Novoselov, and A. K. Geim, Science **360**, 1339 (2018).
[4] Y. Wu and N. R. Aluru, J. Phys. Chem. B **117**, 8802 (2013).
[5] G. Tocci, L. Joly, and A. Michaelides, Nano Lett. **14**, 6872 (2014).
[6] R. P. Misra and D. Blankschtein, J. Phys. Chem. C **121**, 28166 (2017).
[7] J. G. Brandenburg, A. Zen, M. Fitzner, B. Ramberger, G. Kresse, T. Tsatsoulis, A. Grüneis, A. Michaelides, and D. Alfè, J. Phys. Chem. Lett. **10**, 358 (2019).
[8] G. Monet, F. Bresme, A. Kornyshev, and H. Berthoumieux, Phys. Rev. Lett. **126**, 216001 (2021).
[9] N. Kavokine, M.-L. Bocquet, and L. Bocquet, Nature (London) **602**, 84 (2022).
[10] S. Faucher *et al.*, J. Phys. Chem. C **123**, 21309 (2019).
[11] L. Bocquet, Nat. Mater. **19**, 254 (2020).
[12] N. Kavokine, R. R. Netz, and L. Bocquet, Annu. Rev. Fluid Mech. **53**, 377 (2021).
[13] A. Siria, P. Poncharal, A.-L. Biance, R. Fulcrand, X. Blase, S. T. Purcell, and L. Bocquet, Nature (London) **494**, 455 (2013).
[14] A. Esfandiar, B. Radha, F. C. Wang, Q. Yang, S. Hu, S. Garaj, R. R. Nair, A. K. Geim, and K. Gopinadhan, Science **358**, 511 (2017).
[15] J. Comtet, A. Niguès, V. Kaiser, B. Coasne, L. Bocquet, and A. Siria, Nat. Mater. **16**, 634 (2017).
[16] T. Mouterde, A. Keerthi, A. R. Poggioli, S. A. Dar, A. Siria, A. K. Geim, L. Bocquet, and B. Radha, Nature (London) **567**, 87 (2019).
[17] M. Salanne, B. Rotenberg, K. Naoi, K. Kaneko, P.-L. Taberna, C. P. Grey, B. Dunn, and P. Simon, Nat. Energy **1**, 16070 (2016).
[18] A. Siria, M.-L. Bocquet, and L. Bocquet, Nat. Rev. Chem. **1**, 0091 (2017).
[19] D. L. McCaffrey, S. C. Nguyen, S. J. Cox, H. Weller, A. P. Alivisatos, P. L. Geissler, and R. J. Saykally, Proc. Natl. Acad. Sci. U.S.A. **114**, 13369 (2017).

[20] P. Iamprasertkun, W. Hirunpinyopas, A. Keerthi, B. Wang, B. Radha, M. A. Bissett, and R. A. W. Dryfe, J. Phys. Chem. Lett. **10**, 617 (2019).

[21] R. P. Misra and D. Blankschtein, J. Phys. Chem. C **125**, 2666 (2021).

[22] L. Scalfi, M. Salanne, and B. Rotenberg, Annu. Rev. Phys. Chem. **72**, 189 (2021).

[23] C. D. Williams, J. Dix, A. Troisi, and P. Carbone, J. Phys. Chem. Lett. **8**, 703 (2017).

[24] C. Zhan, M. R. Ceron, S. A. Hawks, M. Otani, B. C. Wood, T. A. Pham, M. Stadermann, and P. G. Campbell, Nat. Commun. **10**, 4858 (2019).

[25] M. Ruggeri, K. Reeves, T.-Y. Hsu, G. Jeanmairet, M. Salanne, and C. Pierleoni, J. Chem. Phys. **156**, 094709 (2022).

[26] B. Grosjean, M.-L. Bocquet, and R. Vuilleumier, Nat. Commun. **10**, 1656 (2019).

[27] L. Joly, R. H. Meißner, M. Iannuzzi, and G. Tocci, ACS Nano **15**, 15249 (2021).

[28] C. Y. Son and Z.-G. Wang, Proc. Natl. Acad. Sci. U.S.A. **118**, e2020615118 (2021).

[29] L. Scalfi, T. Dufils, K. G. Reeves, B. Rotenberg, and M. Salanne, J. Chem. Phys. **153**, 174704 (2020).

[30] A. Schlaich, D. Jin, L. Bocquet, and B. Coasne, Nat. Mater. **21**, 237 (2022).

[31] R. P. Misra and D. Blankschtein, Langmuir **37**, 722 (2021).

[32] J. Schwinger, in *Classical Electrodynamics* (CRC Press, Taylor & Francis Group, Boca Raton, 2018).

[33] P. Loche, C. Ayaz, A. Schlaich, D. J. Bonthuis, and R. R. Netz, J. Phys. Chem. Lett. **9**, 6463 (2018).

[34] M. A. Vorotyntsev and A. A. Kornyshev, Zh. Eksp. Teor. Fiz. **72**, 1008 (1980), http://www.jetp.ras.ru/cgi-bin/dn/e_051_03_0509.pdf.

[35] A. A. Kornyshev and M. A. Vorotyntsev, Surf. Sci. **101**, 23 (1980).

[36] A. M. Gabovich, M. S. Li, H. Szymczak, and A. I. Voitenko, Surf. Sci. **606**, 510 (2012).

[37] See Supplemental Material at http://link.aps.org/supplemental/10.1103/PhysRevLett.130.076201 for a detailed description of theoretical framework and response function derivation.

[38] X. Li, J. Feng, E. Wang, S. Meng, J. Klimeš, and A. Michaelides, Phys. Rev. B **85**, 085425 (2012).

[39] L. Hedin and S. Lundqvist, Solid State Phys. **23**, 1 (1970).

[40] F. Giustino, Rev. Mod. Phys. **89**, 015003 (2017).

[41] H. J. C. Berendsen, J. R. Grigera, and T. P. Straatsma, J. Phys. Chem. **91**, 6269 (1987).

[42] R. Kubo, Rep. Prog. Phys. **29**, 255 (1966).

[43] G. Jeanmairet, M. Levesque, R. Vuilleumier, and D. Borgis, J. Phys. Chem. Lett. **4**, 619 (2013).

[44] G. Jeanmairet, N. Levy, M. Levesque, and D. Borgis, J. Phys. Condens. Matter **28**, 244005 (2016).

[45] P. A. Bopp, A. A. Kornyshev, and G. Sutmann, Phys. Rev. Lett. **76**, 1280 (1996).

[46] J.-P. Hansen and I. R. McDonald, *Theory of Simple Liquids* (Academic Press, New York, 2013).

[47] D. J. Bonthuis, S. Gekle, and R. R. Netz, Langmuir **28**, 7679 (2012).

[48] T. Werder, J. H. Walther, R. L. Jaffe, T. Halicioglu, and P. Koumoutsakos, J. Phys. Chem. B **107**, 1345 (2003).

[49] A. H. Castro Neto, F. Guinea, N. M. R. Peres, K. S. Novoselov, and A. K. Geim, Rev. Mod. Phys. **81**, 109 (2009).

[50] G. D. Mahan, *Many-Particle Physics* (Springer, New York, 1990).

[51] E. H. Hwang and S. Das Sarma, Phys. Rev. B **75**, 205418 (2007).

[52] D. Bohm and D. Pines, Phys. Rev. **92**, 609 (1953).

[53] V. Kaiser, J. Comtet, A. Niguès, A. Siria, B. Coasne, and L. Bocquet, Faraday Discuss. **199**, 129 (2017).

[54] Using $N_{\mathrm{ext}}[z] = J_0[q\sqrt{b^2 + (z - z_0)^2}]/2b$ with J_0 being the zeroth-order Bessel function, we compute $F(z_0) = \frac{1}{2}\int_0^{+\infty} \frac{dq}{2\pi} q[N_{\mathrm{ext}}^{\dagger}(W - V)N_{\mathrm{ext}}](q)$, for the three Green's functions, in log-log space using $q = e^{y}E_F/v_F$, $y \in [-1, 8]$, and $N_y = 100$ for convergence. Note that $V[z,z'] = e^{-q|z-z'|}/2\epsilon_0 q$.

[55] L. Scalfi and B. Rotenberg, Proc. Natl. Acad. Sci. U.S.A. **118**, e2108769118 (2021).

[56] Y. Marcus, Chem. Rev. **109**, 1346 (2009).

[57] https://github.com/anton-smirnov-robert/pmf_water_graphene.